A&A 530, A30 (2011)
DOI: 10.1051/0004-6361/201016178

Astronomy & Astrophysics

Lopsidedness in WHISP galaxies

II. Morphological lopsidedness⋆

J. van Eymeren[1], E. Jütte[2], C. J. Jog[3], Y. Stein[2], and R.-J. Dettmar[2]

[1] Fakultät für Physik, Universität Duisburg-Essen, Lotharstr. 1, 47048 Duisburg, Germany
e-mail: janine.vaneymeren@uni-due.de
[2] Astronomisches Institut der Ruhr-Universität Bochum, Universitätsstr. 150, 44780 Bochum, Germany
e-mail: eva.juette@astro.rub.de
[3] Department of Physics, Indian Institute of Science, 560012 Bangalore, India
e-mail: cjjog@physics.iisc.ernet.in

Received 22 November 2010 / Accepted 19 March 2011

ABSTRACT

The distribution of stars and gas in many galaxies is asymmetric. This so-called lopsidedness is expected to significantly affect the dynamics and evolution of the disc, including the star formation activity. Here, we measure the degree of lopsidedness for the gas distribution in a selected sample of 70 galaxies from the Westerbork H I Survey of Spiral and Irregular Galaxies. This complements our earlier work (Paper I) where the kinematic lopsidedness was derived for the same galaxies. The morphological lopsidedness is measured by performing a harmonic decomposition of the surface density maps. The amplitude of lopsidedness A_1, the fractional value of the first Fourier component, is typically quite high (about 0.1) within the optical disc and has a constant phase. Thus, lopsidedness is a common feature in galaxies and indicates a global mode. We measure A_1 out to typically one to four optical radii, sometimes even further. This is, on average, four times larger than the distance to which lopsidedness was measured in the past using near-IR as a tracer of the old stellar component, and therefore provides a new, more stringent constraint on the mechanism for the origin of lopsidedness. Interestingly, the value of A_1 saturates beyond the optical radius. Furthermore, the plot of A_1 versus radius shows fluctuations that we argue are due to local spiral features. We also try to explain the physical origin of this observed disc lopsidedness. No clear trend is found when the degree of lopsidedness is compared to a measure of the isolation or interaction probability of the sample galaxies. However, this does not rule out a tidal origin if the lopsidedness is long-lived. In addition, we find that the early-type galaxies tend to be more morphologically lopsided than the late-type galaxies. Both results together indicate that lopsidedness has a tidal origin.

Key words. surveys – galaxies: evolution – galaxies: ISM – galaxies: structure

1. Introduction

It is now known that both the stellar and the gas distribution in galaxies are often "lopsided", as first highlighted in the classic paper by Baldwin et al. (1980). Rix & Zaritsky (1995) analysed near-IR images of a sample of galaxies and characterised lopsidedness by the $m = 1$ mode of a Fourier analysis. Since then, studies of larger samples of galaxies have been carried out that show that the fraction of lopsided galaxies is quite high and can be 50% or more (Richter & Sancisi 1994; Matthews et al. 1998; Bournaud et al. 2005a; Angiras et al. 2006, 2007). Thus, lopsidedness is common, yet its properties have not been as well-studied as other common asymmetries such as spiral arms or bars, which can be characterised by the $m = 2$ mode.

Lopsidedness can have a significant influence on the evolution of the host galaxy (for a review of lopsided galaxies see, e.g., Jog & Combes 2009). In particular, since the $m = 1$ mode has no inner Lindblad resonance, this mode allows the transport of matter to the central region (Block et al. 1994). Thus, lopsidedness can affect the star formation and play a potential role in fuelling the nuclear region, e.g., an AGN (Reichard et al. 2008).

The high fraction of galaxies showing lopsidedness indicates that it is sustainable over a large period of time. However, its physical origin is still poorly understood. Several mechanisms might be responsible for the observed lopsided discs. Possible scenarios include tidal interactions and minor mergers (Jog 1997; Schoenmakers et al. 1997; Zaritsky & Rix 1997; Bournaud et al. 2005b), asymmetric gas accretion (Bournaud et al. 2005a; Mapelli et al. 2008), ram pressure from the intergalactic medium (Mapelli et al. 2008), but also an offset of the stellar disc in a halo potential (Noordermeer et al. 2001).

Lopsidedness has been found to be correlated with some properties of the galaxies. For instance, Angiras et al. (2006) and Angiras et al. (2007) indicate that the fraction of lopsidedness depends on the environment. A high-density group environment seems to favour the occurrence of lopsided discs. Furthermore, Bournaud et al. (2005a) found a correlation with galaxy type, with late-type discs being more frequently lopsided than early-types. In contrast, the group studies of Angiras et al. (2006) show that the early-type galaxies are more lopsided than late-types which indicates that tidal encounters may be the origin of lopsidedness.

The physical origin of lopsidedness and its lifetime are interrelated and remain poorly understood. A simple kinematic model gives a lifetime of $<10^9$ years (Baldwin et al. 1980).

⋆ Appendix A is available in electronic form at
http://www.aanda.org

A tidal origin that accounts for the self-gravity of the disc gives a somewhat longer time of 1–2 Gyr (Bournaud et al. 2005a). A global mode treatment implies that lopsidedness is very long-lived, about the Hubble time (Saha et al. 2007), although a non-zero pattern speed would make it less long-lived (Jog & Combes 2009).

To place some constraints on the physical origin of lopsidedness, we present a new study of a large sample of disc galaxies. Thanks to several large H I surveys carried out in the past few years, the number of available and useful H I maps has increased enormously. We use deep medium-resolution H I maps of 70 galaxies from the Westerbork H I Survey of Irregular and SPiral galaxies (WHISP[1]). The advantage of using H I instead of near-IR observations is that lopsidedness can be measured to much larger radii, where lopsidedness is more pronounced (Rix & Zaritsky 1995). Owing to the low column density limit of the WHISP data, we have been able to measure the lopsidedness beyond the optical radius in almost all 70 galaxies.

In a previous paper (van Eymeren et al. 2011, hereafter Paper I), the rotation curves of all sample galaxies are presented and the kinematic lopsidedness is analysed by comparing the receding and approaching sides. Here, we complement the results from this kinematic analysis with a study of morphological lopsidedness at all radii.

This paper is organised as follows. In Sect. 2, we briefly mention the sample selection (a more detailed description can be found in Paper I). In Sect. 3, we describe our harmonic analysis. The results are presented in Sect. 4 and discussed in Sect. 5. We summarise the main results and conclusions in Sect. 6.

2. Sample selection

We selected 70 disc galaxies from the WHISP survey by applying two selection criteria: (1) the galaxies need to have inclinations between 20° and 75°, otherwise, the tilted-ring analysis will not work properly; (2) the ratio of the H I diameter to the beam size has to be larger than ten to be able to measure lopsidedness to large radii. To combine reasonably high spatial resolution with sufficiently high signal-to-noise ratio, we worked on data cubes smoothed to a resolution of $30'' \times 30''$. As Fig. 1 in Paper I shows, the selection criteria do not bias our sample: the galaxies are distributed over a large range of B magnitudes and morphological types. They typically extend from one to four optical radii, sometimes even further.

A more detailed description of the selection process and some general properties of the final sample galaxies are given in Paper I. Details of the WHISP survey and the data reduction process can be found in Swaters et al. (2002).

3. Harmonic analysis

The data analysis is based on routines within the Groningen Image Processing System (GIPSY[2], van der Hulst et al. 1992). A tilted-ring analysis to derive the kinematic parameters was performed in Paper I. We concentrate here on describing the harmonic decomposition, which gives us quantitative values of the morphological lopsidedness, and the calculation of the halo perturbation.

[1] http://www.astro.rug.nl/~whisp/
[2] http://www.astro.rug.nl/~gipsy/

3.1. Morphological lopsidedness of the H I gas

The amplitude of lopsidedness in the morphology was calculated by decomposing the H I surface density map into Fourier components

$$\sigma(R,\phi) = a_0(R) + \sum a_m(R)\cos(m\phi - \phi_m(R)), \quad (1)$$

where $a_0(R)$ is the mean surface density at a given radius R, a_m is the amplitude of the surface density harmonic coefficient, ϕ is the azimuthal angle in the plane of the galaxy, and ϕ_m is the phase of the mth Fourier coefficient. This harmonic decomposition was carried out with the GIPSY task *reswri* by using the best-fit kinematic parameters derived in Paper I. We note that all pixels within an annular ring are treated equally, which means that any small-scale structure is averaged out. The amplitudes were obtained up to the third Fourier component. We then calculated the normalised harmonic coefficients $A_m = a_m/a_0$, where A_1 represents the normalised amplitude of the $m = 1$ Fourier component denoting lopsidedness, whereas A_2 represents the amplitude of an $m = 2$ component denoting a bar or a two-armed spiral feature.

It is crucial to accurately determine the dynamic centre and keep it (and the systemic velocity) fixed for all rings because if x_0, y_0, and $v_{\rm sys}$ are allowed to vary, the $m = 2$ harmonic coefficients tend to rearrange themselves to minimise the effects of lopsidedness. In Paper I, we showed that the optical and dynamic centre usually agree within one beam size.

3.2. Lopsidedness due to a perturbed halo

We assume that the asymmetry arises because of the response of the disc to a halo distorted by a tidal encounter (Jog 1997). The perturbation potential can then be obtained from the H I surface density maps using the normalised amplitudes A_1, A_2, and A_3 for $m = 1$, $m = 2$, and $m = 3$, respectively, as obtained for an exponential disc (Jog 2000).

In agreement with Angiras et al. (2006), we found that the H I radial surface density profiles were in most cases roughly Gaussian in cross-section. Therefore, we derived the Gaussian scale length for all sample galaxies. A radial surface density profile was first obtained from the H I surface density maps. We then fitted a Gaussian curve of $S_0\ \exp(-(R-b)^2/2R_{\rm w}^2)$ to the profiles using a χ^2 fitting technique (GIPSY task *gauprof*).

The relation between ϵ_1, the perturbation parameter for the lopsided potential, and A_1 for a radial Gaussian distribution (see Angiras et al. 2006) is given by

$$\epsilon_1 = \frac{A_1(R)}{2\left(\frac{R}{R_{\rm w}}\right)^2 - 1}, \quad (2)$$

where $A_1(R)$ is the morphological lopsidedness and $R_{\rm w}$ is the Gaussian scale length.

The corresponding relations for $m = 2$ and $m = 3$ are given by

$$\epsilon_2 = \frac{A_2(R)}{\left(\frac{R}{R_{\rm w}}\right)^2 + 1}, \quad (3)$$

and

$$\epsilon_3 = \frac{A_3(R)}{(2/7)\left(\frac{R}{R_{\rm w}}\right)^2 + 1}, \quad (4)$$

4. Results

4.1. Morphological lopsidedness

Figure 1 shows plots of the amplitude $A_1(R)$ and the phase $\phi_1(R)$ of lopsidedness vs. R/R_{25}, where R_{25} is the apparent radius of the optical disc. Most galaxies in our sample have H I data extending beyond R_{25} (see Fig. 1, Paper I). Therefore, the Fourier analysis is performed beyond the optical radius and in some cases to several times this distance. The optical disc size, R_{25} is typically equal to four to five times the exponential disc scale length (van der Kruit & Searle 1982). Thus, in the present paper, the A_1 values denoting the lopsided amplitude are measured to four or more disc scale lengths. This is much larger than the maximum distance of 2.5 disc scale lengths to which lopsidedness can be studied in the near-IR (Rix & Zaritsky 1995; Bournaud et al. 2005a), where this limit is set by the high sky background.

Previous studies showed that in the region within the optical disc, A_1 increases with radius (Rix & Zaritsky 1995; Saha et al. 2007). This trend was also seen in the H I studies of the Eridanus group galaxies that covered about four disc scale lengths or the optical radius (Angiras et al. 2006). In contrast, we find here that only about 20% of our sample galaxies display a steady increase in the morphological lopsidedness towards large radii. Good examples are UGC 2455, UGC 4173, or UGC 4278. There are also examples of galaxies where the values of $A_1(R)$ scatter significantly with radius (e.g., UGC 2953 or UGC 7989). In other galaxies, we discovered pronounced features such as those found in UGC 3851 or UGC 7353. Finally, we also detected galaxies with a constant value of $A_1(R)$ (e.g., UGC 3574 or UGC 7081).

We consider R_{25} to be the limiting radius between the inner and the outer disc. We therefore calculated a mean value of the amplitude $A_1(R)$ over all radii smaller than R_{25} and all radii larger than R_{25}. The results are given in Table 1, in Cols. 4 and 5. The last line shows the mean of the averaged amplitudes over all sample galaxies. The mean $\langle A_1 \rangle$ for large radii is about 0.15, and for small radii about 0.11, which means that the inner parts of our sample galaxies are on average slightly less perturbed than the outer parts. All sample galaxies showing amplitudes above these values are considered lopsided. For large radii, we found 30 galaxies with strong signs of lopsidedness, 38 galaxies having values below 0.15 (for two galaxies, we only have data within R_{25}). For small radii, about 50% of all sample galaxies are strongly lopsided.

We note that the typical lopsided amplitude A_1 within the optical disc ($R < R_{25}$) of about 0.11 agrees with the value obtained by Bournaud et al. (2005a) for the inner half of the optical disc (1.5–2.5 optical disc scale lengths) from near-IR studies of the OSU sample. Angiras et al. (2006) studied the H I asymmetry in 18 galaxies of the Eridanus group and obtained a mean larger than 0.2 in this radial range. Therefore, our WHISP sample shows less lopsidedness than a group case.

As we discussed in Paper I, the existence of warps might affect the determination of the lopsidedness, especially of low to moderately inclined galaxies. However, this effect is not likely to be more pronounced at large radii. This is because the amplitudes of both of these features increase with radius. Furthermore, the amplitude of lopsidedness appears to saturate at radii beyond the optical disc.

A striking result from Fig. 1 is that the phase $\phi_1(R)$ is nearly constant with radius, which indicates that $m = 1$ is a global mode. We note that $\phi_1(R)$ is given in radians. The apparently different values are the same angle modulo 2ϕ. This result will be discussed in detail in Sect. 5.2.

4.2. A comparison of $\langle A_1 \rangle$, $\langle A_2 \rangle$, and $\langle A_3 \rangle$

We now wish to compare the mean normalised amplitudes averaged over $R/R_{25} > 1$ and $R/R_{25} < 1$ for the first three Fourier components of the H I surface density distribution. The upper two panels in Fig. 2 show $\langle A_2 \rangle$ vs. $\langle A_1 \rangle$ averaged over large and small radii. We see a comparable distribution for large radii, whereas at small radii, the $m = 2$ perturbations are much stronger. As mentioned in Sect. 3.1, A_2 denotes perturbations caused by a bar or spiral arms. Although spiral arms can be found at all radii in a disc, bars will dominate in the central parts. This shows that the amplitudes of the $m = 2$ mode are comparable to those of the $m = 1$ mode at large radii, but clearly dominate at small radii. $\langle A_3 \rangle$ is generally smaller than $\langle A_1 \rangle$ independent of the radial range we consider (Fig. 2, lower panels).

We calculated the mean of A_1, A_2, and A_3 for the two different radial ranges: confirming the results from the graphs, the mean of A_2 is lower than the mean of A_1 for all radii. The mean of A_3 is lower for all radii (see Table 1).

4.3. Lopsided potential

As shown in Sect. 3.2, we can derive the perturbation of the halo up to third order from the parameters for the morphological lopsidedness. The values are given in the last three columns of Table A.1. For completeness reasons we also list the values of the fractional Fourier amplitudes A_1, A_2, and A_3 between one and two Gaussian scale lengths in Table A.1. We calculated the mean of all parameters. In agreement with the results for the morphological lopsidedness (see Table A.1, Cols. 2 to 4), the mean of $\langle \epsilon_2 \rangle$ is higher than the mean of $\langle \epsilon_1 \rangle$, whereas the mean of $\langle \epsilon_3 \rangle$ is slightly lower than the mean of $\langle \epsilon_2 \rangle$.

5. Discussion

5.1. Variation in lopsidedness with radius

As mentioned in Sect. 4.1, a pronounced increase in the morphological lopsidedness is only found in about 20% of all sample galaxies. This is somewhat surprising as near-IR observations at smaller radii show that an increase in A_1 with radius seems to be a common feature in disc galaxies (Rix & Zaritsky 1995). Here, the neutral gas can be traced out to several times the apparent optical radius R_{25}. At these large radii, the increase in A_1 does not continue, but appears to saturate. The origin of this difference is poorly understood, but it provides an important clue to the origin of the disc lopsidedness at large radii. Unfortunately, a direct comparison of the behaviours of the stellar and gaseous components cannot be done here since the inner parts of the galaxies, on which scales Rix & Zaritsky (1995) found an increase in lopsidedness, are not resolved in our H I maps.

To obtain a clearer picture, we selected two galaxies and compared their global profiles, the H I morphology, and the distributions of A_1 and ϕ_1 with radius. UGC 4173 (see Fig. 3, upper row) is a galaxy where we found the expected behaviour of increasing lopsidedness with radius. As can be seen, the H I distribution is quite smooth with a clear asymmetry in the south-east. UGC 7256 (Fig. 3, lower row) is an example of a galaxy where we found strong fluctuations, so-called wiggles, in the distribution of A_1. The H I intensity map shows a spiral galaxy with pronounced arms. The global profile has two typical maxima. However, the intensities of the peaks differ slightly from each other, indicating lopsidedness. Furthermore, in both cases the phase $\phi_1(R)$ is nearly constant with radius, which is indicative

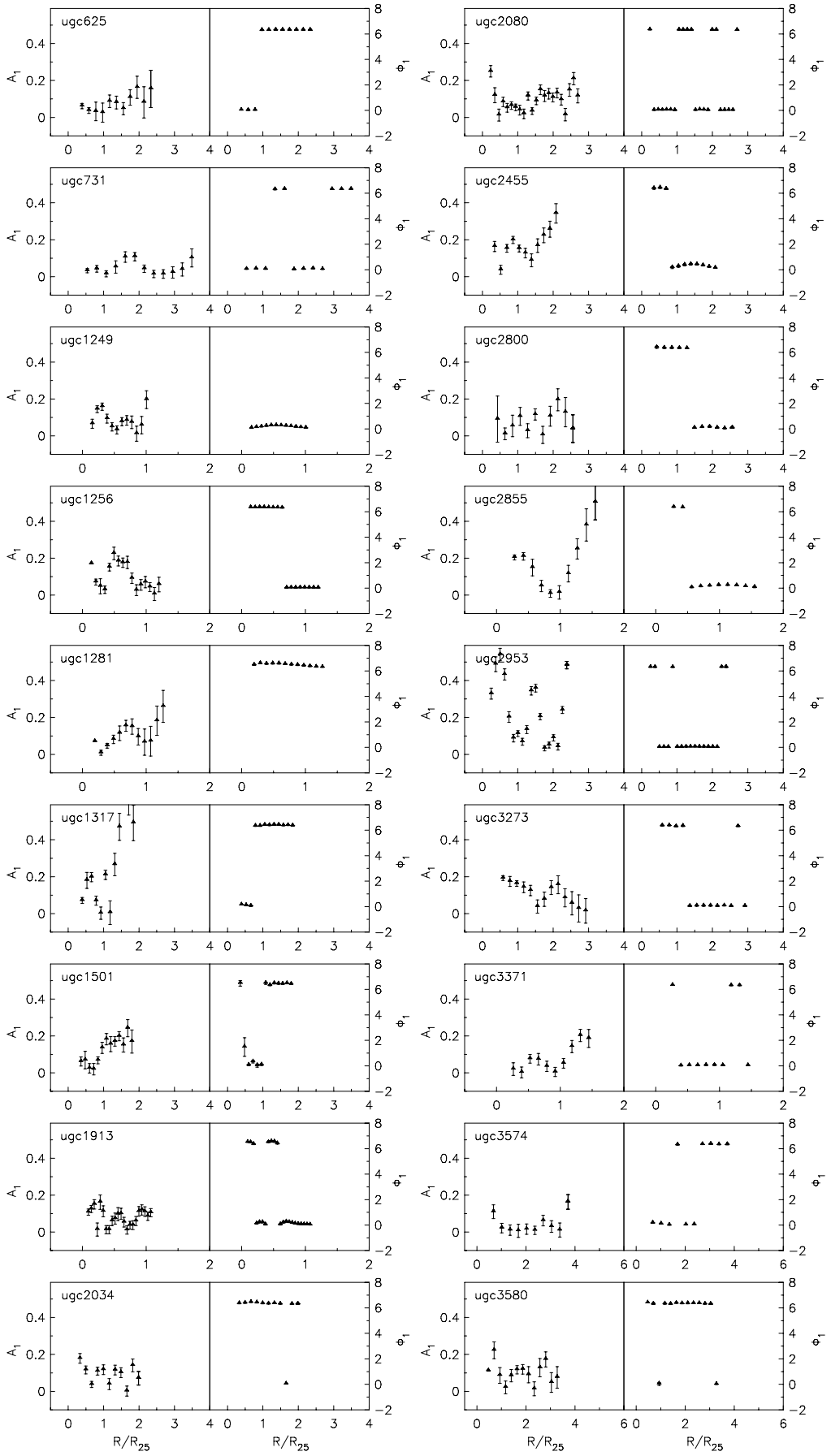

Fig. 1. *Left panels*: morphological lopsidedness A_1 as a function of R/R_{25}; *right panels*: phase ϕ_1 as a function of R/R_{25}.

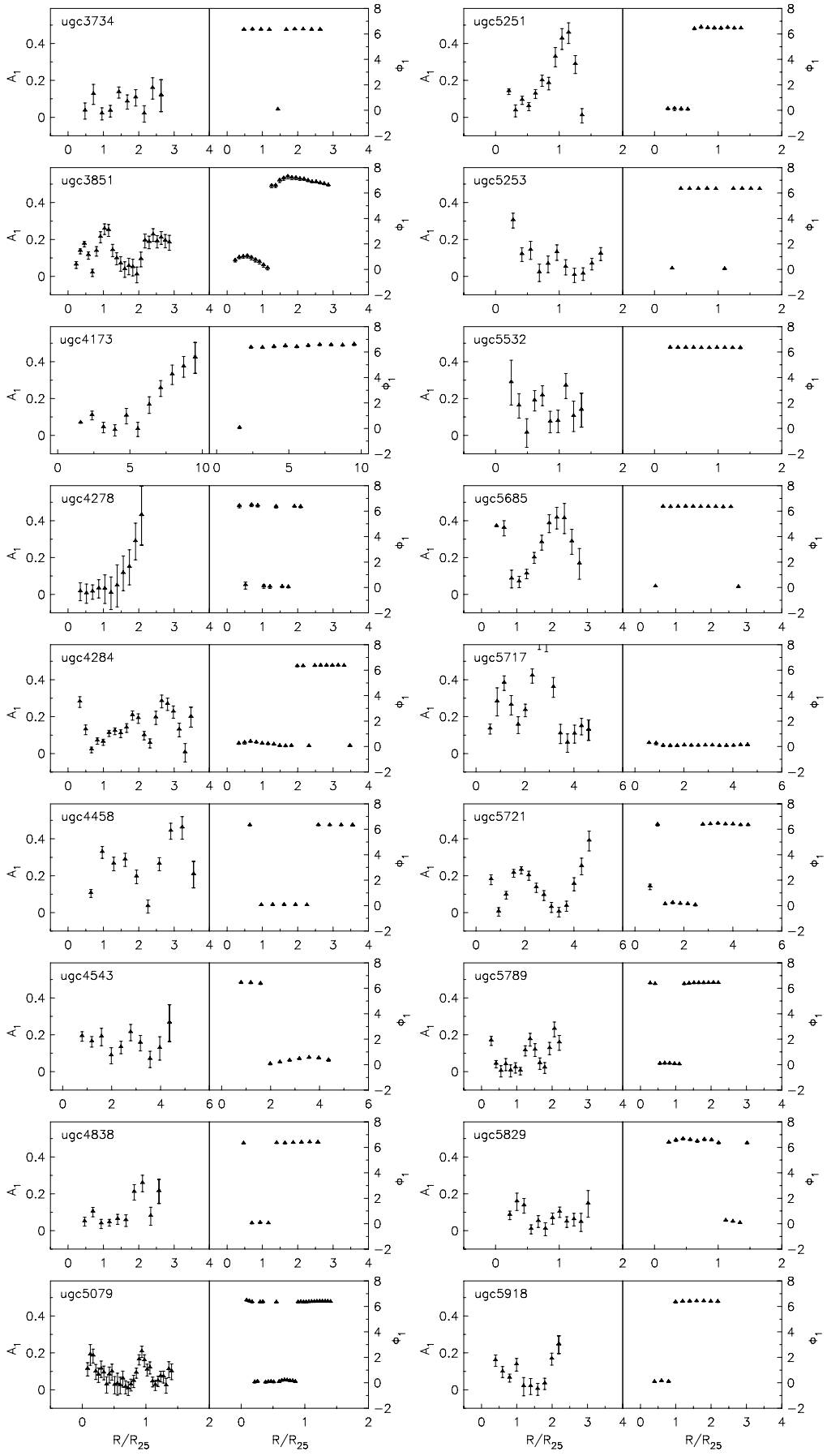

Fig. 1. continued.

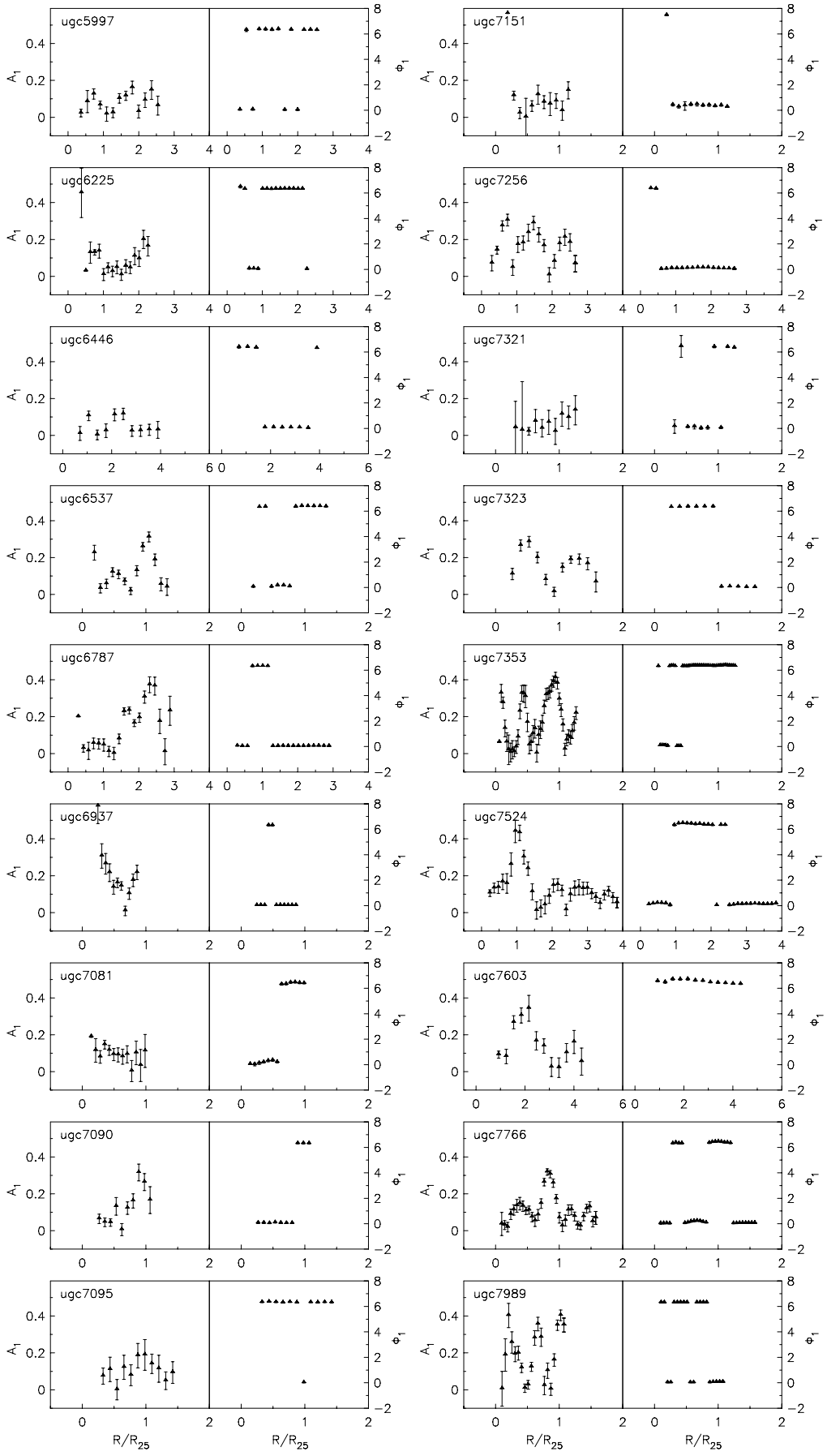

Fig. 1. continued.

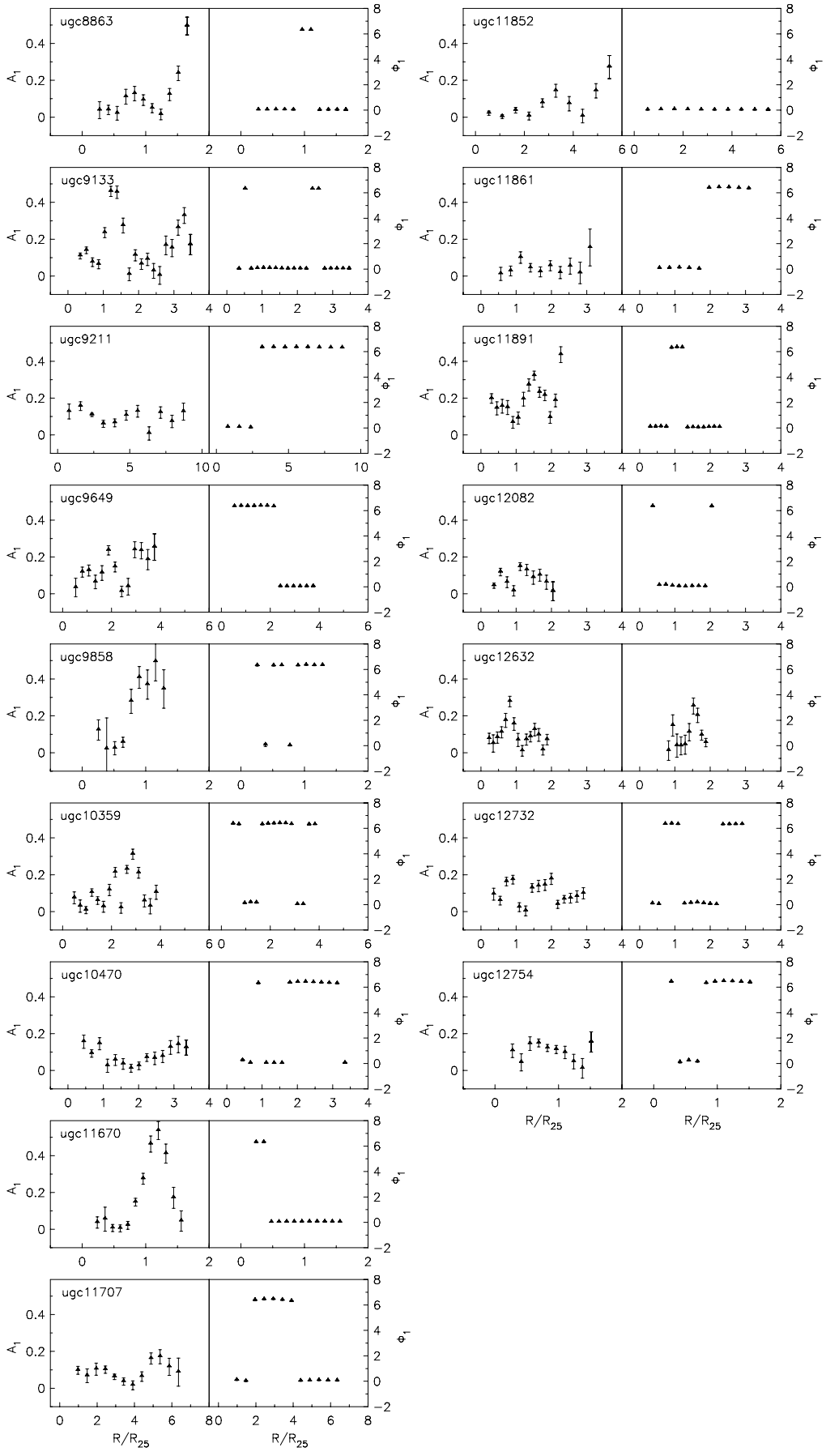

Fig. 1. continued.

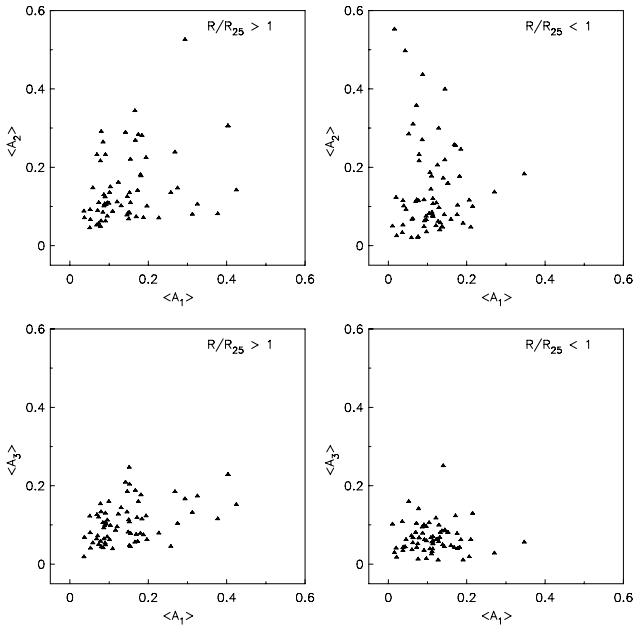

Fig. 2. A comparison of the mean values of the fractional amplitudes of the first three Fourier components of the H I surface density distribution. *Upper row*: $\langle A_2 \rangle$ vs. $\langle A_1 \rangle$ for large and small radii, beyond and within the optical radius, respectively. The $\langle A_2 \rangle$ values denoting bars and two-armed spirals dominate over lopsidedness within the optical radius, for amplitudes >0.2. Thus, strong bars are more likely in the inner galaxy than very strong lopsidedness. *Lower row*: $\langle A_3 \rangle$ vs. $\langle A_1 \rangle$ for large and small radii, the $\langle A_3 \rangle$ values are smaller than lopsided amplitudes, especially at large radii.

of a global $m = 1$ mode. We therefore suggest that the fluctuations in the distribution of A_1 reflect the local H I morphology (i.e., local spiral arms) superposed on top of the global lopsidedness.

A natural way to explain the origin of these local spiral features would be via the swing amplification (Goldreich & Lynden-Bell 1965; Toomre 1981). These fluctuations are not apparent in the near-IR studies that measure the asymmetry in the underlying old stellar distribution (see, e.g., Fig. 1 in Rix & Zaritsky 1995). This might be because a low dispersion component such as gas has a stronger amplitude for the swing amplification feature than stars (Jog 1992). This is true even in the linear regime studied in the above swing amplification papers, and in a real galaxy the gas will be more likely to undergo an additional non-linear growth in its amplitude.

We verified whether this overall picture is reasonable. If the galaxy rotation curve displays a linear increase with radius, i.e., when it denotes a region of solid body rotation so that the angular speed is constant, the swing amplification idea cannot work. Hence, the net A_1 is then likely to be a pure underlying global $m = 1$ component showing a radial increase in the lopsided amplitude. This is confirmed exactly for galaxies such as UGC 4173 or UGC 4278, which display a smooth radial increase in A_1 (Fig. 2) and have solid body rotation in the corresponding radial regions as seen in Fig. A1, Paper I. In contrast, in the region of the flat rotation curve, the differential rotation is significant and the swing amplification is effective, resulting in the fluctuations as found for UGC 731 or UGC 2080, which have a flat rotation curve (Fig. A1, Paper I) and a fluctuating A_1 in the same radial region (Fig. 1). Since flat rotation curves are common, this explains why most of our sample galaxies show fluctuations in the amplitude for lopsidedness A_1 in H I.

We note that while the lopsided amplitude A_1 displays large, local fluctuations, its overall value increases with radius linearly up to the optical radius and then more gradually at larger radii. Thus, we can explain why lopsidedness was first noted in H I in the outer parts of galaxies such as M 101 (Baldwin et al. 1980). Therefore, H I still serves as an excellent tracer of lopsidedness in the outer galactic discs.

Figure 4 shows the distribution of $\langle A_1 \rangle$ for small (dotted histogram) and large radii (solid histogram). Surprisingly, both distributions are comparable: most galaxies have a lopsidedness parameter below 0.2, only a few having higher values. Thus, while the lopsidedness is lower in the inner parts than beyond the optical disc (Table 1), the increase is not strong and the A_1 values seem to saturate beyond the optical radius. This needs to be studied by future theoretical work.

5.2. The phase $\phi_1(R)$

In Sect. 4.1, we showed that the phase $\phi_1(R)$ is in most cases nearly constant with radius. This trend was already noted for smaller samples studied to a radial extent smaller than the optical radius (Rix & Zaritsky 1995; Angiras et al. 2007). The phase remains remarkably constant even when the lopsided amplitude shows a wide variation with radius as discussed above. This indicates that $m = 1$ is a global mode and represents a perturbation in the underlying mass distribution. Since the stars typically contribute less than the gas to the surface density beyond the optical radius or about four to five disc scale lengths as in our Galaxy (Narayan & Jog 2002), the constant phase most likely denotes the origin of the lopsided potential to be the distorted dark matter halo, to which the H I in the outer disc responds. This confirms our assumption made in deriving the perturbation potential (Sect. 3.2). It also implies that gas accretion is less likely to be the underlying mechanism of lopsidedness, which was proposed by Bournaud et al. (2005a).

5.3. Morphological vs. kinematic lopsidedness

Kinematic and morphological asymmetries have been argued to be causally connected (Jog 2002). However, Kornreich et al. (2002) showed that both asymmetries are not always correlated. We therefore wish to determine how kinematic and morphological lopsidedness are correlated in the WHISP sample.

A comparison of $\epsilon_{\rm kin}$ and $\langle \epsilon_1 \rangle$, the perturbation parameter in the lopsided potential obtained by analysing the kinematic and morphological data, respectively, is presented in Fig. 5. Following the classification in Paper I, we distinguish five kinematic classes:

- *Type 1*: the receding and approaching sides agree on all scales (solid triangles);
- *Type 2*: constant offset of the receding and approaching sides (solid squares);
- *Type 3*: differences between the receding and approaching sides only at large radii (open triangles);
- *Type 4*: differences between the receding and approaching sides only at small radii (open squares);
- *Type 5*: the receding and approaching sides change sides (stars).

In general, the perturbation parameters calculated from the morphological and kinematic data can be seen to be comparable.

Table 1. Lopsidedness parameters.

UGC	Hubble type	R_{25} [kpc]	$\langle A_1 \rangle$ $(>1R/R_{25})$	$\langle A_1 \rangle$ $(<1R/R_{25})$	$\langle A_2 \rangle$ $(>1R/R_{25})$	$\langle A_2 \rangle$ $(<1R/R_{25})$	$\langle A_3 \rangle$ $(>1R/R_{25})$	$\langle A_3 \rangle$ $(<1R/R_{25})$	T_p
(1)	(2)	(3)	(4)	(5)	(6)	(7)	(8)	(9)	(10)
625	4	13.94	0.103	0.039	0.148	0.099	0.096	0.041	−5.88
731	9.9	2.17	0.052	0.037	0.090	0.048	0.078	0.040	...
1249	8.9	7.05	0.197	0.077	0.099	0.112	0.061	0.139	−2.81
1256	6	7.42	0.036	0.114	0.086	0.105	0.017	0.049	−2.68
1281	7.5	4.10	0.171	0.088	0.779	0.434	0.117	0.077	...
1317	4.9	23.33	0.425	0.104	0.140	0.080	0.150	0.103	...
1501	7.8	3.46	0.181	0.063	0.176	0.308	0.174	0.065	...
1913	7	14.52	0.096	0.079	0.107	0.214	0.110	0.065	−5.46
2034	9.8	4.43	0.078	0.112	0.214	0.080	0.056	0.030	−6.80
2080	6	8.50	0.101	0.091	0.134	0.047	0.060	0.033	...
2455	9.9	3.27	0.194	0.138	0.223	0.045	0.121	0.047	...
2800	10	7.02	0.091	0.052	0.103	0.283	0.128	0.158	...
2855	5	9.03	0.312	0.106	0.078	0.185	0.13	0.037	...
2953	3.4	8.74	0.180	0.347	0.179	0.181	0.077	0.054	...
3273	9	4.56	0.087	0.177	0.128	0.101	0.090	0.038	...
3371	9.9	7.08	0.146	0.036	0.076	0.031	0.131	0.106	...
3574	5.8	4.69	0.037	0.110	0.069	0.175	0.066	0.024	−8.70
3580	1.1	5.97	0.087	0.140	0.099	0.170	0.062	0.249	...
3734	4.4	4.83	0.092	0.059	0.103	0.018	0.100	0.070	...
3851	9.8	2.16	0.142	0.121	0.287	0.049	0.207	0.115	...
4173	9.9	1.54	0.175	...	0.281	...	0.158	...	...
4278	6.4	4.40	0.151	0.016	1.213	0.550	0.245	0.027	−4.99
4284	6	4.30	0.155	0.111	0.108	0.083	0.076	0.055	−7.05
4458	1	14.46	0.268	0.215	0.237	0.098	0.183	0.127	...
4543	7.9	5.55	0.154	0.191	0.218	0.055	0.043	0.008	...
4838	5.2	11.59	0.131	0.062	0.100	0.066	0.142	0.052	...
5079	4	15.25	0.071	0.087	0.087	0.268	0.070	0.093	...
5251	4.3	14.97	0.294	0.144	0.524	0.397	0.164	0.084	−4.90
5253	2.4	11.14	0.051	0.129	0.043	0.095	0.120	0.097	−5.21
5532	3.9	24.35	0.169	0.144	0.072	0.217	0.074	0.085	...
5685	4	6.78	0.258	0.271	0.133	0.134	0.043	0.026	−6.74
5717	3.7	6.49	0.275	0.206	0.145	0.114	0.102	0.017	−7.41
5721	6.6	1.58	0.152	0.091	0.081	0.115	0.105	0.098	...
5789	6	7.44	0.109	0.045	0.085	0.090	0.037	0.061	...
5829	9.8	5.85	0.079	0.072	0.061	0.115	0.131	0.041	...
5918	10	2.81	0.080	0.113	0.290	0.075	0.042	0.037	...
5997	4	8.17	0.084	0.075	0.083	0.019	0.103	0.050	...
6225	6	7.18	0.074	0.176	0.108	0.077	0.048	0.076	−7.92
6446	6.6	2.46	0.052	0.011	0.064	0.048	0.039	0.100	...
6537	5.1	10.92	0.149	0.114	0.081	0.072	0.080	0.068	−5.71
6787	1.7	9.53	0.173	0.070	0.139	0.110	0.056	0.079	−5.50
6937	4	20.24	...	0.210	...	0.045	...	0.060	−3.47
7081	4.7	13.60	...	0.097	...	0.073	...	0.094	−3.32
7090	5.3	8.67	0.166	0.129	0.342	0.298	0.054	0.055	−6.65
7095	4.1	11.57	0.099	0.109	0.106	0.142	0.158	0.065	−6.86
7151	6	2.67	0.091	0.125	0.061	0.204	0.047	0.062	−6.32
7256	−2.7	8.33	0.167	0.168	0.267	0.255	0.186	0.041	...
7321	6.6	5.01	0.116	0.043	0.738	0.495	0.084	0.042	...
7323	7.9	4.48	0.152	0.160	0.133	0.065	0.202	0.045	−5.67
7353	4	19.46	0.146	0.185	0.123	0.244	0.183	0.060	−2.40
7524	8.9	2.12	0.121	0.182	0.109	0.175	0.093	0.041	−8.00
7603	7	1.60	0.152	0.092	0.082	0.061	0.046	0.061	...
7766	6	19.84	0.073	0.137	0.0551	0.047	0.118	0.082	−6.00
7989	2.2	25.91	0.377	0.171	0.079	0.254	0.113	0.121	−3.85
8863	1	14.36	0.184	0.072	0.279	0.355	0.113	0.102	−8.15
9133	2.4	22.77	0.188	0.097	0.070	0.064	0.073	0.012	...
9211	9.9	1.16	0.095	0.127	0.073	0.060	0.067	0.008	...
9649	3	2.08	0.150	0.076	0.066	0.021	0.111	0.011	...
9858	4	21.61	0.403	0.152	0.304	0.157	0.226	0.079	−6.54
10359	5.6	4.86	0.124	0.037	0.159	0.051	0.126	0.033	...
10470	4	6.90	0.069	0.131	0.230	0.038	0.124	0.066	...
11670	0.5	7.70	0.325	0.078	0.104	0.231	0.172	0.065	...
11707	8	2.37	0.090	0.097	0.122	0.033	0.052	0.057	...
11852	1	10.61	0.085	0.021	0.262	0.023	0.039	0.015	...

Table 1. continued

UGC	Hubble type	R_{25} [kpc]	$\langle A_1 \rangle$ $(>1R/R_{25})$	$\langle A_1 \rangle$ $(<1R/R_{25})$	$\langle A_2 \rangle$ $(>1R/R_{25})$	$\langle A_2 \rangle$ $(<1R/R_{25})$	$\langle A_3 \rangle$ $(>1R/R_{25})$	$\langle A_3 \rangle$ $(<1R/R_{25})$	T_p
(1)	(2)	(3)	(4)	(5)	(6)	(7)	(8)	(9)	(10)
11861	7.8	6.49	0.058	0.020	0.145	0.121	0.052	0.039	...
11891	9.9	4.33	0.227	0.143	0.069	0.077	0.077	0.043	...
12082	8.8	3.95	0.091	0.060	0.230	0.065	0.105	0.035	−6.71
12632	8.7	4.28	0.068	0.133	0.050	0.056	0.062	0.079	−6.24
12732	8.7	5.29	0.089	0.123	0.105	0.107	0.097	0.061	−6.35
12754	6	4.70	0.078	0.114	0.047	0.118	0.152	0.057	−5.99
mean	...	...	0.148	0.111	0.177	0.136	0.105	0.063	...

Notes. (1) Galaxy name from the UGC catalogue; (2) morphological type following the classification by de Vaucouleurs (1979); (3) apparent radius from the HyperLeda database; (4) to (9) the mean values of the parameters for morphological lopsidedness obtained in this paper; (10) tidal parameter derived from Eq. (5).

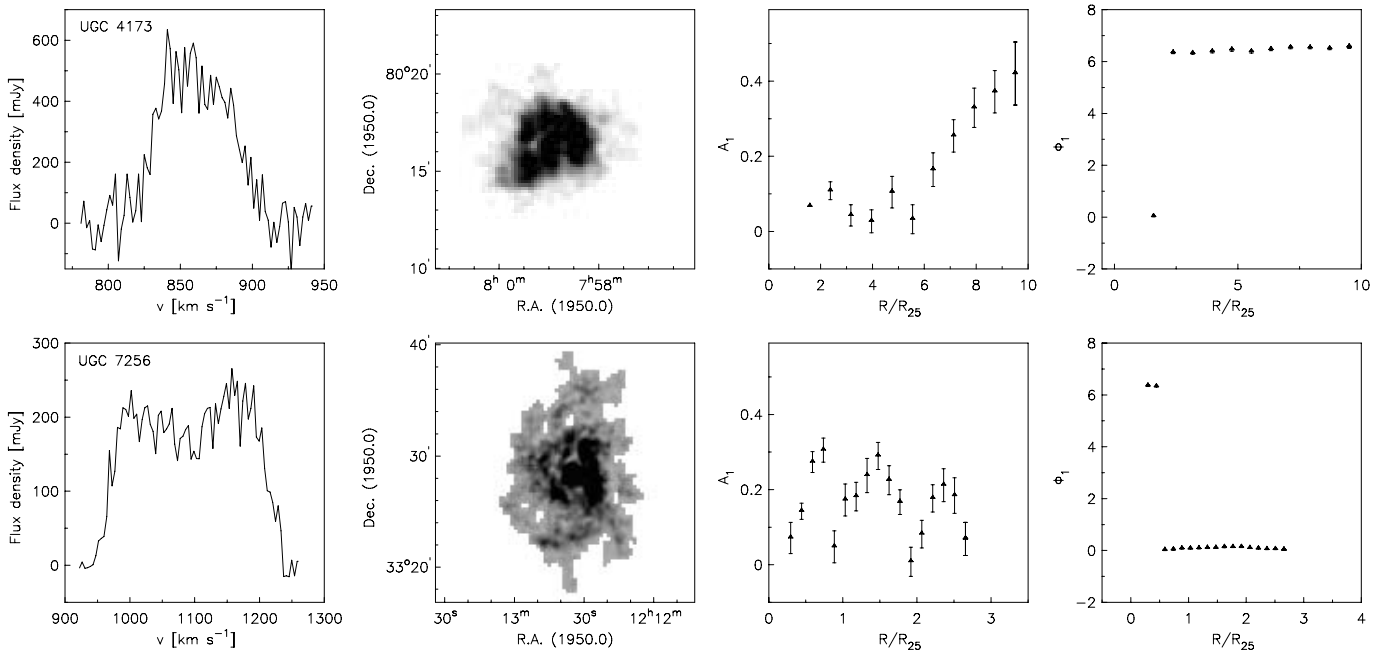

Fig. 3. Global profile (*left panels*), H I intensity distribution and the distribution of A_1 (*middle panels*), and the distribution of the phase ϕ_1 (*right panels*) of two example galaxies, UGC 4173 (*upper row*) and UGC 7256 (*lower row*).

There are a few cases where galaxies show a much higher value for $\epsilon_{\rm kin}$ than for $\epsilon_{\rm I}$ (UGC 1249, UGC 2034, UGC 2080, UGC 4458, UGC 4543). These galaxies are all classified as type 2. For UGC 2034, the rotation velocity could not be well defined because the rotation curve shows a second rise at higher radii. We took an average value of the first plateau as a lower limit to $v_{\rm rot}$, which results in an upper limit to $\epsilon_{\rm kin}$. For UGC 2080, we did not find any local asymmetries in the velocity field, but only a global offset to the iso-velocity contours (see Paper I, Sect. 4.1). This results in a high $\epsilon_{\rm kin}$, while the galaxy is only moderately lopsided morphologically. Thus, the way that the lopsidedness is measured may produce a spurious discrepancy between kinematic and morphological lopsidedness in some galaxies. The same seems to be true for the other three galaxies.

There are also a few cases where the perturbation parameter obtained from the morphological data is higher than the one obtained from the kinematic data. A good example is UGC 8863 (Paper I, Sect. 4.1), where the perturbation parameter derived from the kinematic data is small because differences between the receding and approaching sides are small in the outer parts where the maximum rotation velocities have been measured. The perturbation parameter obtained from the morphological data, however, is much higher.

We can conclude that morphological and kinematic lopsidedness are generally comparable, which is in good agreement with Jog (2002).

5.4. Tidal origin of lopsidedness

As mentioned in the introduction, the physical origin of lopsidedness and its lifetime are closely connected, i.e., different mechanisms lead to different lifetimes of lopsidedness. We study here the correlations of A_1 with galaxy type and the strength of the tidal interaction. As A_1 was measured to very large distances, we can constrain the mechanism behind the origin of lopsidedness more reliably than in earlier studies.

In a first step, we compare the morphological lopsidedness $\langle A_1 \rangle$ averaged over large and small radii (Fig. 6, left and right panels, respectively) to the morphological type. The early-type

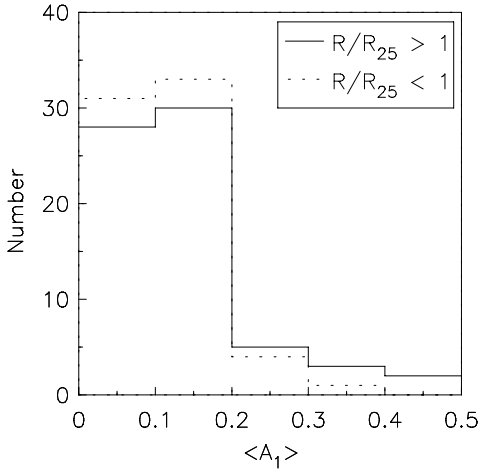

Fig. 4. The distribution of $\langle A_1 \rangle$ for small (dotted histogram) and large radii (solid histogram).

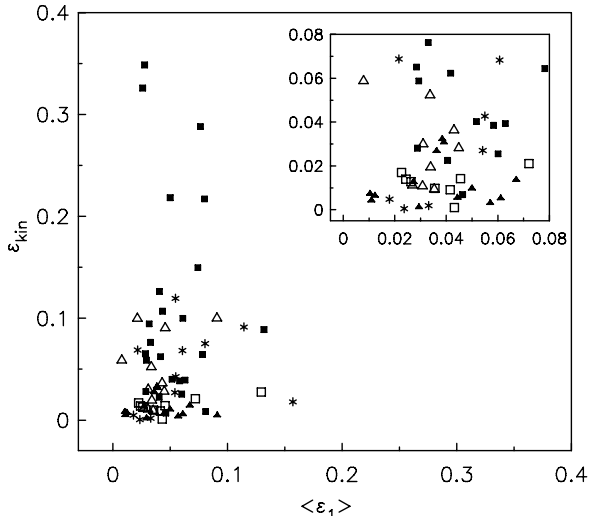

Fig. 5. The perturbation parameter in the lopsided potential obtained by the analysis of the kinematic data $\langle \epsilon_{\rm kin} \rangle$ vs. the one obtained from the morphological data $\langle \epsilon_1 \rangle$. The symbols represent the five kinematic classes defined in Paper I. Type 1: receding/approaching sides agree on all scales (solid triangles); type 2: constant offset of receding/approaching sides (solid squares); type 3: differences only at large radii (open triangles); type 4: differences only at small radii (open squares); type 5: receding and approaching sides change sides (stars).

spiral galaxies seem to be more strongly lopsided, especially in the outer radial regions. Since a tidal interaction drives a galaxy towards being an early-type, this high lopsidedness in early-type galaxies indicates that tidal encounters are the mechanism responsible for lopsidedness (see also Angiras et al. 2006).

As a next step, we consider the environment of our sample galaxies. The degree of lopsidedness depends on the distance between the main galaxy and its companions, as well as on the mass ratio of the main galaxy to its companions. We therefore use the so-called tidal parameter to quantify the effect of tidal forces (Bournaud et al. 2005a), which is given by

$$T_{\rm p} = \log\left(\sum_i \frac{M_i}{M_0}\left(\frac{R_0}{D_i}\right)^3\right), \quad (5)$$

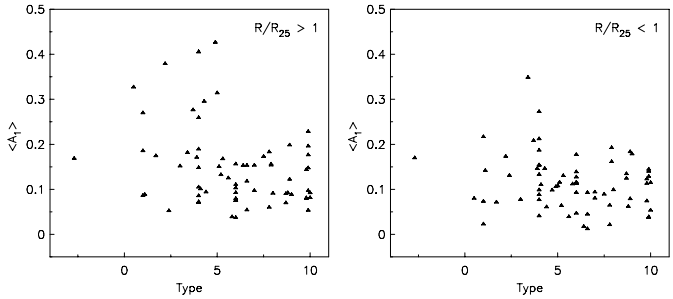

Fig. 6. Morphological lopsidedness vs. morphological type for large (*left panel*) and small (*right panel*) radii.

where M_i is the mass of each companion, M_0 is the mass of the main galaxy, R_0 is the scale length, and D_i is the distance of each companion from the main galaxy. The ratio of the masses is estimated from the ratio of absolute blue magnitudes. We take $R_{25}/4$ as an estimate of the exponential disc scale length (van der Kruit & Searle 1982). We searched for neighbours using the Tully Nearby Galaxies Catalogue (Tully & Fisher 1988). We only include companions within a radius of 2.5° and with measured radial velocities within 500 km s^{-1}. Although almost all galaxies in our sample are members of groups or associations, many of them appear to be isolated on the basis of the above-mentioned criteria. We find 31 galaxies to have between 1 and 15 companions. The $T_{\rm p}$ values of these 31 galaxies are plotted in Fig. 7 vs. the parameter for morphological lopsidedness $\langle A_1 \rangle$ averaged over large radii (large filled triangles). In a few cases, up to two companions do not have any data for the absolute blue magnitude, which gives us a lower limit to the tidal parameter (large open triangles). In two cases, only data within R_{25} are available so that we show $\langle A_1 \rangle$ for small radii (small open triangles). We also plot the remaining 39 galaxies, for which no companion is known. This makes them very isolated, which is expressed by the assumed low tidal parameter of −10. As can be seen, these galaxies display the whole range of values for $\langle A_1 \rangle$.

In good agreement with Bournaud et al. (2005a), we have found no correlation between $\langle A_1 \rangle$ and $T_{\rm p}$. Strong lopsidedness is as common in more isolated galaxies (smaller $T_{\rm p}$) as in galaxies with many companions. This implies that there has to be a different, internal mechanism producing lopsidedness in isolated galaxies to cause them to be lopsided. Alternatively, if the lopsidedness is long-lived as indicated by theoretical studies (Saha et al. 2007), or if it is caused by satellite accretion as proposed by Zaritsky & Rix (1997) and shown by simulations (Bournaud et al. 2005a), then these two factors could explain why isolated galaxies could also be lopsided. If lopsidedness were long-lived, then there would be no correlation of A_1 with a tidal parameter even if the origin of lopsidedness is a tidal encounter. As shown above, the greater lopsidedness seen in early-type galaxies (Fig. 6) is indicative there of a tidal origin. Thus, these two points together indicate that a tidal encounter is the likely origin of lopsidedness in the WHISP sample studied here.

We note that this analysis is limited by the incompleteness of the Tully Nearby Galaxies Catalogue. In some cases, not all relevant parameters were listed in the catalogue so that these companions could not be included in the tidal parameter calculation. Furthermore, it is likely that not all small companions have been detected so far. This method provides a good indicator of the overall local environment of the galaxies, even though some low-mass companions might be missing.

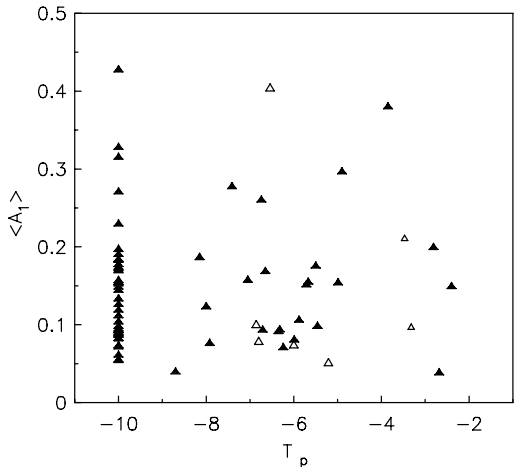

Fig. 7. The amplitude of morphological lopsidedness $\langle A_1 \rangle$ averaged over large radii vs. the tidal parameter T_p (large filled triangles). In some cases, up to two companions could not be included in the calculation of T_p because of a lack of data. This gives a lower limit to T_p (large open triangles). In two cases, the H I emission could only be detected within R_{25} so that $\langle A_1 \rangle$ averaged over small radii is plotted vs. T_p (small open triangles). For all galaxies which have no known companions, a tidal parameter of −10 is assumed. There is no clear correlation of the lopsided amplitude with the tidal parameter.

6. Summary

We have carried out a harmonic analysis of the H I surface density distribution and measured the morphological lopsidedness of 70 galaxies selected from the WHISP survey. The amplitude of lopsidedness, A_1, is defined to be the fractional amplitude of the first azimuthal Fourier component. The most interesting aspect of this study is that the high sensitivity data enable us to measure lopsidedness for the first time out to large radial distances. Lopsidedness is typically measured to between one and four optical radii and in a very few cases even ten optical radii (Fig. 1, Paper I).

The main results of our study can be summarised as follows:

- The mean amplitude of lopsidedness, $\langle A_1 \rangle$ within the optical disc is large, about 0.1. The values of A_1 increase radially within this radial range. Beyond the optical disc, the values seem to saturate.
- The phase is remarkably constant with radius indicating that the lopsidedness is a global mode, as previously argued (Saha et al. 2007).
- In a few cases, the values of A_1 increase with radius, but in most cases display small-scale fluctuations. We have argued that the latter are due to local spiral features arising from swing amplification.
- As shown in Paper I, the galaxies can be divided into five groups based on their rotation velocity patterns. The most common types are galaxies whose velocity fields are globally distorted (types 2 and 5). In general, the extents of the kinematic and morphological lopsidedness agree quite well.
- Early-type galaxies seem to be more lopsided than late-typegalaxies. We did not find a correlation between lopsidedness and the tidal parameter indicating the strength of interactions for the sample galaxies.

The results from both the morphological and kinematic studies indicate that tidal encounters are the main mechanism responsible for the halo lopsidedness, to which the disc responds.

Acknowledgements. The authors would like to thank the anonymous referee for the constructive feedback which helped to improve this paper.
We wish to thank Thijs van der Hulst for providing us with the WHISP data cubes before they became publicly available. C.J. would like to thank DFG (Germany) and INSA (India) for supporting a visit to Germany in October 2007 under INSA-DFG Exchange Programme, during which this collaboration was initiated. We made use of NASA's Astrophysics Data System (ADS) Bibliographic Services and the NASA/IPAC Extragalactic Database (NED) which is operated by the Jet Propulsion Laboratory, California Institute of Technology, under contract with the National Aeronautics and Space Administration. We acknowledge the usage of the HyperLeda database (http://leda.univ-lyon1.fr).

References

Angiras, R. A., Jog, C. J., Omar, A., & Dwarakanath, K. S. 2006, MNRAS, 369, 1849
Angiras, R. A., Jog, C. J., Dwarakanath, K. S., & Verheijen, M. A. W. 2007, MNRAS, 378, 276
Baldwin, J. E., Lynden-Bell, D., & Sancisi, R. 1980, MNRAS, 193, 313
Block, D. L., Bertin, G., Stockton, A., et al. 1994, A&A, 288, 365
Bournaud, F., Combes, F., Jog, C. J., & Puerari, I. 2005a, A&A, 438, 507
Bournaud, F., Jog, C. J., & Combes, F. 2005b, A&A, 437, 69
de Vaucouleurs, G. 1979, ApJ, 227, 380
Goldreich, P., & Lynden-Bell, D. 1965, MNRAS, 130, 125
Jog, C. J. 1992, ApJ, 390, 378
Jog, C. J. 1997, ApJ, 488, 642
Jog, C. J. 2000, ApJ, 542, 216
Jog, C. J. 2002, A&A, 391, 471
Jog, C. J., & Combes, F. 2009, Phys. Rep., 471, 75
Kornreich, D. A., Lovelace, R. V. E., & Haynes, M. P. 2002, ApJ, 580, 705
Mapelli, M., Moore, B., & Bland-Hawthorn, J. 2008, MNRAS, 388, 697
Matthews, L. D., van Driel, W., & Gallagher, III, J. S. 1998, AJ, 116, 1169
Narayan, C. A., & Jog, C. J. 2002, A&A, 394, 89
Noordermeer, E., Sparke, L. S., & Levine, S. E. 2001, MNRAS, 328, 1064
Reichard, T. A., Heckman, T. M., Rudnick, G., Brinchmann, J., & Kauffmann, G. 2008, ApJ, 677, 186
Richter, O., & Sancisi, R. 1994, A&A, 290, L9
Rix, H., & Zaritsky, D. 1995, ApJ, 447, 82
Saha, K., Combes, F., & Jog, C. J. 2007, MNRAS, 382, 419
Schoenmakers, R. H. M., Franx, M., & de Zeeuw, P. T. 1997, MNRAS, 292, 349
Swaters, R. A., van Albada, T. S., van der Hulst, J. M., & Sancisi, R. 2002, A&A, 390, 829
Toomre, A. 1981, in Structure and Evolution of Normal Galaxies, ed. S. M. Fall, & D. Lynden-Bell, 111
Tully, R. B., & Fisher, J. R. 1988, Catalog of Nearby Galaxies, ed. R. B. Tully, & J. R. Fisher
van der Hulst, J. M., Terlouw, J. P., Begeman, K. G., Zwitser, W., & Roelfsema, P. R. 1992, in Astronomical Data Analysis Software and Systems I, ed. D. M. Worrall, C. Biemesderfer, & J. Barnes, ASP Conf. Ser., 25, 131
van der Kruit, P. C., & Searle, L. 1982, A&A, 110, 61
van Eymeren, J., Jütte, E., Jog, C. J., Stein, Y., & Dettmar, R.-J. 2011, A&A, 530, A29
Zaritsky, D., & Rix, H. 1997, ApJ, 477, 118

Pages 13 to 15 are available in the electronic edition of the journal at http://www.aanda.org

Appendix A: Lopsided potential

We present the perturbation parameters in the lopsided potential derived from the morphological data up to the third Fourier component. We also provide the Gaussian scale lengths, the parameters for morphological lopsidedness up to third order, and the perturbation parameter in the lopsided potential obtained from the kinematic data in Paper I.

Table A.1. Lopsidedness parameters.

UGC	R_w [kpc]	$\langle A_1 \rangle$ $(1 < R_w < 2)$	$\langle A_2 \rangle$ $(1 < R_w < 2)$	$\langle A_3 \rangle$ $(1 < R_w < 2)$	$\langle \epsilon_{kin} \rangle$	$\langle \epsilon_1 \rangle$ $(1 < R_w < 2)$	$\langle \epsilon_2 \rangle$ $(1 < R_w < 2)$	$\langle \epsilon_3 \rangle$ $(1 < R_w < 2)$
(1)	(2)	(3)	(4)	(5)	(6)	(7)	(8)	(9)
625	16.35	0.106	0.157	0.107	0.065	0.029	0.052	0.058
731	3.38	0.051	0.060	0.073	0.001	0.029	0.020	0.043
1249	3.77	0.076	0.151	0.138	0.326	0.026	0.054	0.084
1256	4.68	0.078	0.084	0.056	0.005	0.044	0.030	0.037
1281	2.36	0.109	0.588	0.098	0.009	0.050	0.192	0.062
1317	20.61	0.355	0.139	0.141	0.008	0.081	0.047	0.095
1501	2.62	0.152	0.291	0.126	0.091	0.046	0.100	0.070
1913	6.67	0.064	0.238	0.083	0.013	0.026	0.070	0.055
2034	4.80	0.078	0.214	0.056	0.349	0.028	0.064	0.033
2080	14.01	0.119	0.134	0.051	0.218	0.050	0.042	0.034
2455	2.88	0.152	0.260	0.062	0.107	0.043	0.069	0.037
2800	9.24	0.098	0.106	0.138	0.011	0.031	0.026	0.071
2855	6.93	0.154	0.123	0.099	0.019	0.034	0.047	0.061
2953	17.30	0.214	0.309	0.098	0.028	0.130	0.138	0.073
3273	5.63	0.104	0.149	0.048	0.009	0.035	0.047	0.027
3371	5.63	0.118	0.064	0.114	0.028	0.029	0.017	0.065
3574	7.91	0.025	0.061	0.061	0.059	0.008	0.021	0.036
3580	9.39	0.098	0.087	0.057	0.030	0.039	0.022	0.037
3734	6.62	0.102	0.118	0.108	0.126	0.041	0.034	0.061
3851	2.89	0.116	0.301	0.214	0.052	0.034	0.081	0.136
4173	8.01	0.262	0.432	0.225	0.150	0.074	0.128	0.138
4278	3.41	0.028	1.218	0.050	0.007	0.010	0.391	0.031
4284	7.53	0.168	0.134	0.078	0.005	0.061	0.041	0.047
4458	21.16	0.243	0.303	0.144	0.217	0.080	0.079	0.077
4543	14.73	0.164	0.307	0.065	0.288	0.076	0.103	0.041
4838	15.80	0.145	0.100	0.149	0.007	0.046	0.030	0.094
5079	10.21	0.075	0.162	0.085	0.014	0.024	0.062	0.053
5251	9.19	0.286	0.612	0.161	0.100	0.091	0.201	0.096
5253	15.79	0.094	0.029	0.040	0.100	0.061	0.013	0.029
5532	21.52	0.146	0.056	0.086	0.039	0.063	0.018	0.058
5685	10.24	0.324	0.119	0.051	0.091	0.115	0.040	0.032
5717	16.47	0.265	0.155	0.100	0.018	0.157	0.047	0.060
5721	4.23	0.136	0.089	0.143	0.062	0.042	0.033	0.090
5789	7.55	0.085	0.067	0.047	0.012	0.027	0.025	0.032
5829	3.69	0.055	0.058	0.096	0.005	0.018	0.021	0.056
5918	3.47	0.092	0.309	0.044	0.100	0.022	0.096	0.028
5997	10.79	0.102	0.092	0.125	0.026	0.036	0.025	0.075
6225	8.63	0.084	0.100	0.053	0.017	0.023	0.031	0.032
6446	6.39	0.027	0.067	0.044	0.006	0.012	0.026	0.030
6537	8.09	0.143	0.077	0.080	0.027	0.054	0.027	0.052
6787	12.07	0.216	0.126	0.072	0.039	0.058	0.042	0.047
6937	13.74	0.165	0.080	0.111	0.003	0.091	0.032	0.079
7081	6.11	0.077	0.042	0.079	0.059	0.029	0.015	0.047
7090	5.24	0.173	0.426	0.062	0.120	0.055	0.146	0.039
7095	8.74	0.122	0.148	0.134	0.040	0.052	0.054	0.085
7151	1.69	0.091	0.113	0.034	0.032	0.038	0.041	0.021
7256	10.96	0.176	0.288	0.180	0.075	0.081	0.093	0.108
7321	3.06	0.070	0.6900	0.061	0.011	0.027	0.222	0.034
7323	3.25	0.131	0.077	0.138	0.010	0.036	0.022	0.075
7353	9.70	0.225	0.273	0.065	0.043	0.055	0.097	0.039
7524	3.58	0.102	0.087	0.083	0.002	0.033	0.028	0.051
7603	2.57	0.196	0.101	0.046	0.064	0.078	0.031	0.028
7766	13.34	0.141	0.039	0.180	0.068	0.061	0.012	0.112
7989	11.17	0.151	0.356	0.115	0.001	0.043	0.107	0.067
8863	11.53	0.107	0.195	0.081	0.009	0.042	0.058	0.049
9133	42.66	0.138	0.071	0.087	0.028	0.045	0.022	0.053
9211	4.81	0.087	0.080	0.043	0.030	0.031	0.024	0.024
9649	3.59	0.151	0.081	0.116	0.002	0.057	0.024	0.074
9858	15.16	0.380	0.250	0.183	0.089	0.132	0.077	0.111
10359	11.49	0.137	0.226	0.181	0.013	0.067	0.079	0.119
10470	13.52	0.090	0.246	0.113	0.094	0.032	0.071	0.068
11670	4.68	0.289	0.136	0.169	0.026	0.060	0.040	0.094
11707	6.98	0.094	0.178	0.051	0.069	0.022	0.045	0.031
11852	31.10	0.128	0.386	0.047	0.023	0.041	0.104	0.031

Table A.1.

UGC	R_w [kpc]	$\langle A_1 \rangle$ $(1 < R_w < 2)$	$\langle A_2 \rangle$ $(1 < R_w < 2)$	$\langle A_3 \rangle$ $(1 < R_w < 2)$	$\langle \epsilon_{kin} \rangle$	$\langle \epsilon_1 \rangle$ $(1 < R_w < 2)$	$\langle \epsilon_2 \rangle$ $(1 < R_w < 2)$	$\langle \epsilon_3 \rangle$ $(1 < R_w < 2)$
(1)	(2)	(3)	(4)	(5)	(6)	(7)	(8)	(9)
11861	9.59	0.034	0.097	0.047	0.004	0.011	0.031	0.030
11891	4.44	0.203	0.054	0.096	0.021	0.072	0.017	0.059
12082	4.50	0.079	0.239	0.101	0.076	0.033	0.075	0.061
12632	4.25	0.068	0.050	0.068	0.001	0.024	0.017	0.043
12732	7.28	0.106	0.092	0.120	0.036	0.043	0.032	0.074
12754	3.02	0.106	0.042	0.060	0.014	0.046	0.013	0.036
mean	...	0.136	0.191	0.096	0.049	0.049	0.062	0.059

Notes. (1) Galaxy name from the UGC catalogue; (2) Gaussian scale length as measured in this paper; (3) to (5) the mean values of the parameters for morphological lopsidedness averaged between one and two Gaussian scale lengths; (6) the perturbation parameter in the lopsided potential obtained from the kinematic data in Paper I; (7) to (9) the mean values of the perturbation parameters obtained from the morphological data in the present paper.